Biochimica et Biophysica Acta 1838 (2014) 1122–1131

Contents lists available at ScienceDirect

Biochimica et Biophysica Acta

journal homepage: www.elsevier.com/locate/bbamem

MD simulations of the central pore of ryanodine receptors and sequence comparison with 2B protein from coxsackie virus ☆

Roman Schilling [a], Rainer H.A. Fink [a], Wolfgang B. Fischer [b,c,*]

[a] Medical Biophysics Group, Institute of Physiology and Pathophysiology, University of Heidelberg, 69120 Heidelberg, Germany
[b] Institute of Biophotonics, School of Biomedical Science and Engineering, National Yang-Ming University, Taipei 112, Taiwan
[c] Biophotonics & Molecular Imaging Research Center (BMIRC), National Yang-Ming University, Taipei 112, Taiwan

ARTICLE INFO

Article history:
Received 15 July 2013
Received in revised form 16 November 2013
Accepted 12 December 2013
Available online 21 December 2013

Keywords:
Ryanodine receptor
Ca homeostasis
Molecular dynamics simulations
Ion dynamics
Viral channel proteins
2B of coxsackie virus

ABSTRACT

The regulation of intracellular Ca^{2+} triggers a multitude of vital processes in biological cells. Ca^{2+} permeable ryanodine receptors (RyRs) are the biggest known ion channels and play a key role in the regulation of intracellular calcium concentrations, particularly in muscle cells. In this study, we construct a computational model of the pore region of the skeletal RyR and perform molecular dynamics (MD) simulations. The dynamics and distribution of Ca^{2+} around the luminal pore entry of the RyR suggest that Ca^{2+} ions are channeled to the pore entry due to the arrangement of (acidic) amino acids at the extramembrane surface of the protein. This efficient mechanism of Ca^{2+} supply is thought to be part of the mechanism of Ca^{2+} conductance of RyRs. Viral myocarditis is predominantly caused by coxsackie viruses that induce the expression of the protein 2B which is known to affect intracellular Ca^{2+} homeostasis in infected cells. From our sequence comparison, it is hypothesized, that modulation of RyR could be due to replacement of its transmembrane domains (TMDs) by those domains of the viral channel forming protein 2B of coxsackie virus. This article is part of a Special Issue entitled: Viral Membrane Proteins — Channels for Cellular Networking.

1. Introduction

Biological cells possess a Ca^{2+} signaling network that is involved in the regulation of numerous cellular processes. Viruses are capable to modulate the calcium regulation of their host cells for their own purposes [1]. The cytosolic calcium concentration of poliovirus-infected neuroblastoma IMR5 cells is reported to increase, partly due to the release of calcium ions from the endoplasmic reticulum (ER) *via* ryanodine receptors (RyRs) [2]. In cardiac and skeletal muscle cells, RyRs are located in the sarcoplasmic reticulum (SR) membrane and possess a key role in the Ca^{2+} regulation responsible for muscle contraction and other vital processes [3–5]. Upon the depolarization of skeletal muscle fibers voltage dependent calcium channels are activated to gate directly type 1 ryanodine receptors (RyR1). In cardiac cells, depolarization causes a cellular inflow of calcium ions and the process of 'calcium-induced calcium release' (CICR) is induced *via* type 2 ryanodine receptors (RyR2). Calcium ions are released from the SR into the myoplasm where they bind to the troponin–tropomyosin regulatory proteins to enable the myosin–actin interaction and the 'cross-bridge cycling' of force generation.

RyRs are the biggest known ion channels consisting of large ~2 MDa homotetrameric assemblies with ~5000 amino acids per monomer [6]. The best structural information for the entire protein has been obtained by cryo-electron microscopy studies [7–9]. RyRs comprise a larger cytoplasmic region and a smaller transmembrane (TM) region that consists of 6–8 transmembrane domains (TMDs) per monomer [10,11]. Besides their function as calcium channel, RyRs are able to interact with numerous small molecules and other proteins to modulate the release of calcium ions from the SR [6].

An altered calcium homeostasis is found in cells infected by coxsackie virus which is recognized as the predominant cause of viral myocarditis [12,13]. Coxsackie virus belongs to the genus *Enteroviruses* of the family Picornaviridae. Similarly to poliovirus its genome encodes the short hydrophobic protein 2B localized at the SR/ER [13]. It consists of 99 amino acids and harbors two putative TMDs [14] one of which is amphipathic [15]. Polytopic 2B has been identified to increase membrane permeability to calcium ions in the SR/ER and Golgi [16]. Structural features of 2B as a putative bundle forming an ion conducting pore have been suggested by computational modeling [17]. Experimental mutagenesis studies however reveal that there must be additional function of 2B than just rendering the membrane permeable to ions [14].

Several viral channel forming proteins are known to interact with host proteins to modulate cell function for the benefit of viral replication (reviewed in [18]). It is suggested that Vpu of HIV-1 affects the

☆ This article is part of a Special Issue entitled: Viral Membrane Proteins — Channels for Cellular Networking.

* Corresponding author at: Institute of Biophotonics, School of Biomedical Science and Engineering, National Yang-Ming University, 155, Li-Non St., Sec. 2, Taipei, 112, Taiwan. Tel.: +886 2 2826 7394; fax: +886 2 28235460.
E-mail address: wfischer@ym.edu.tw (W.B. Fischer).

0005-2736/$ – see front matter © 2013 Elsevier B.V. All rights reserved.
http://dx.doi.org/10.1016/j.bbamem.2013.12.008

potassium channel TASK [19]. Sequence overlap with the first transmembrane domain (TMD1) of TASK with the TMD of Vpu stimulated the idea that throughout manufacturing of TASK, Vpu could occupy the same position as TMD1 of TASK. As a consequence of this replacement TASK would be malfunctioning by not enabling a change of the electrochemical gradient.

In the present study, we built a pore model of the RyR1 and carry out molecular dynamics (MD) simulations to understand the dynamics of calcium ions when approaching the receptor. Sparked by the above outlined idea the sequence of 2B is aligned with those of the two RyRs predominantly expressed in skeletal and cardiac muscle, RyR1 and RyR2, respectively.

2. Materials and methods

2.1. Modeling of the pore region of the RyR

Since the TM regions of the RyR are putatively located at the C-terminal end [10,11], the sequence T4200–S5037 of the rabbit RyR1 (P11716, www.uniprot.org) was assessed by the TM prediction programs TMHMM2 (www.cbs.dtu.dk) [20], SOSUI (bp.nuap.nagoya-u.ac.jp) [21], SVMtm (ccb.imb.uq.edu.au) [22], Phobius (phobius.sbc.su.se) [23], HMMTOP (www.enzim.hu) [24], OCTOPUS (octopus.cbr.su.se) [25] and MEMSAT-SVM (bioinf.cs.ucl.ac.uk) [26]. The sequence of the putative pore region of the RyR1 was aligned with the sequence of the KvAP potassium channel (PDB ID: 2A0L, www.pdb.org) [27] using ClustalW2 (www.ebi.ac.uk) in its default mode with the exception of gap penalty being set to 'gap open = 50'.

The software suit Molecular Operating Environment (MOE) 2010.10 (www.chemcomp.com) was used to create homology models of the pore region of the RyR1 with the KvAP potassium channel as template. The modeling was performed in three steps building selectivity filter and pore helices first, followed by the generation of inner helices and outer helices. In each step 100 models were created which were scored according to the GB/VI scoring function. The Amber99 force field with a reaction field treatment of solvation electrostatics was used for modeling. The side-chain sampling was performed at 310 K. Energy minimizations were carried out with the MOE suit.

The two luminal loops of the pore region of the RyR1 were modeled by the fragment-based cyclic coordinate descent (CCD) algorithm [28] available in the software suit Rosetta 3.2.1 (www.rosettacommons.org). The required fragment files were generated using the Robetta server (robetta.bakerlab.org). Membrane specific weights of the scoring function and membrane penalty scores were used to account for the membrane environment [29,30]. 2316 loop models connecting selectivity filter and inner helix and 10,000 loop models connecting pore helix and outer helix were built. The Rosetta suit was also used to assign the loop models to different clusters according to the root mean square (RMS) criteria. Only the 20 largest clusters were retained and putative outliners were removed.

The final model was fitted in three cryo-EM density maps (1275, 1606 and 1607, www.emdatabank.org) [7,9] using UCSF Chimera 1.8 (www.cgl.ucsf.edu).

2.2. MD simulations

MD simulations were carried out using GROMACS 4.5.4 (www.gromacs.org) [31]. The created model of the pore region of the RyR1 was embedded in a hydrated and equilibrated POPC bilayer. The program TMDET (tmdet.enzim.hu) [32] was used in order to find an appropriate initial position of the model relative to the membrane. After adding calcium ions to the membrane system the insertion of the pore model was carried out with the tool g_membed [33] from the GROMACS package. The system was submitted to an energy minimization followed by a series of equilibration MD simulations. During a short 50 ps NVT and a 15 ns NPT simulation position restraints with a force constant of 1000 kJ mol^{-1} nm^{-2} were applied to all heavy atoms of the model. Subsequently another 3 ns NPT simulation was conducted applying position restrains only to the backbone atoms of the model. During the following production run of 100 ns only the C_α atoms located in the membrane not including the loop regions were restrained similar to another approach [34]. The entire system comprised of 48,850 atoms (the model of the pore region of the RyR1, 22 calcium ions, 234 lipid and 10,600 water molecules).

The Gromos96 (ffG45a3) force field [35] with additional parameters for lipids [36,37] was used for all MD simulations. The protein, lipid molecules and solvent including ions were coupled separately to the Nosé–Hoover thermostat at a temperature of 310 K and a time constant of 0.5 ps. The Parrinello–Rahman barostat was used for semi-isotropic pressure coupling with a reference pressure of 1 bar, a time constant of 2 ps and a compressibility of $4.5 \cdot 10^{-5}$ bar^{-1}. Long range electrostatic interactions were calculated with the particle-mesh Ewald (PME) method. A cut-off of 1.0 nm for short range electrostatic interactions and 1.4 nm for van der Waals interactions was used.

The trajectory of the last 90 ns of the production run was used for analysis. Two-dimensional calcium ion distributions were computed using g_densmap from the GROMACS package. Spatial distribution functions, distances between calcium ions and protein atoms, the (cumulative) radial distribution function (RDF), the assignment of calcium ions to certain regions and the occupancy of these regions were calculated using self-developed analysis software.

The potential of mean force (PMF) was calculated using umbrella sampling techniques [38–40]. The equilibrated protein membrane system was used as starting configuration. In a steered MD simulation an additional calcium ion (neutralized by two chloride ions) was attached to a spring with a force constant of 2000 kJ mol^{-1} nm^{-2} moving with a

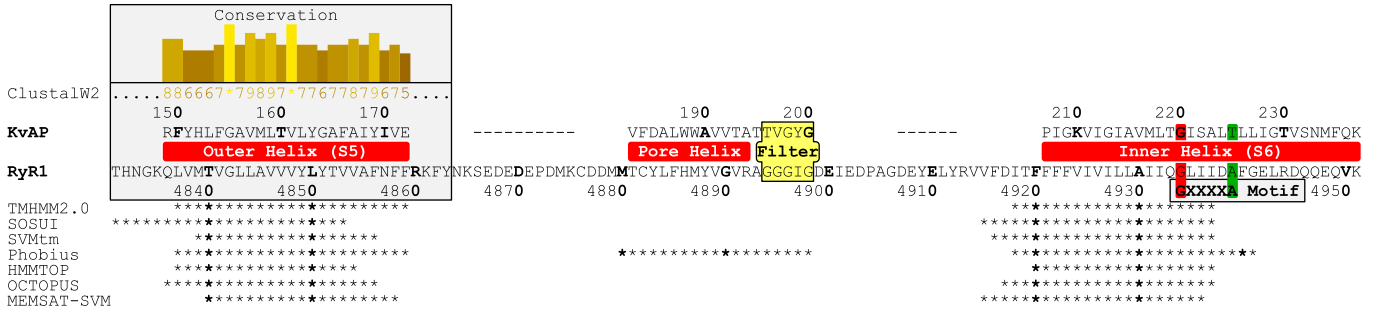

Fig. 1. Sequence alignment of the RyR1 and the KvAP potassium channel. Three separate sequence alignments for the outer helix, pore helix and selectivity filter and inner helix are shown. The outer helix of KvAP is aligned with the putative outer helix of the RyR1 using ClustalW2. The selectivity filter of KvAP is aligned manually with the putative selectivity filter of RyR1. The inner helices of KvAP and RyR1 are aligned manually in order to match Gly-220 of KvAP with Gly-4934 of RyR1 which is part of the GXXXXA motif. Predicted TMDs of RyR1 are labeled with an asterisk.

pull rate of 0.5 nm/ns along the axial direction. Starting configurations for the umbrella sampling windows were extracted in steps of 0.05 nm. Restraining the calcium ion in axial direction with a force constant of 2000 kJ mol^{-1} nm^{-2} every starting configuration was submitted to a 2 ns MD simulation. The compressibility in axial direction was set to zero. Other simulation parameters were identical to those used in the normal MD simulation. The PMF profile was derived from the last 1.5 ns of each simulation using the weighted histogram analysis method (WHAM) implemented in the program g_wham from the GROMACS package [41]. Bootstrap analysis (n = 100) was conducted to estimate the statistical error.

2.3. Sequence analysis

The sequence of the human RyR2 (Q92736, www.uniprot.org) and the sequence of the rabbit RyR1 were aligned using ClustalW2. The TM prediction programs mentioned above were used to identify TMDs in the C-terminal sequence S4155–N4967 of the RyR2 that corresponds to the sequence T4200–S5037 of RyR1. The sequences of the TMDs S37–V54 (TMD1) and L63–W82 (TMD2) of 2B from coxsackie virus [14] and T35–V52 (TMD1) and T61–W80 (TMD2) of 2B from poliovirus [14] were aligned pairwise with the C-terminal sequence of the RyR1 and the RyR2.

Figures were created using PyMOL (www.pymol.org), UCSF Chimera 1.8 (www.cgl.ucsf.edu) and Visual Molecular Dynamics (VMD) (www.ks.uiuc.edu). The trajectories of calcium ions were low-pass filtered for visualization using g_filter from the GROMACS package.

The calculations were run on a DELL studio XPS.

3. Results

3.1. Modeling of the pore region of the RyR

Assessment of the C-terminal sequence of RyR1 by various TM prediction programs indicates two TM regions from approximately T4831–F4859 and V4915–G4941 (Fig. 1) that are likely to correspond to the outer and the inner helices, respectively [7,9,10,42]. The program Phobius also predicts a helical TM stretch within region M4880–G4898. Sequence alignment of the target is done with the sequence of KvAP [27] to build a homology model of the pore region (Fig. 1). The sequence Q4836–F4859 is aligned with the sequence of the outer helix S5 of KvAP (R149–E172) (Fig. 1, boxed). The sequence of the putative selectivity filter of RyR1 (G4894–G4898) [43] is aligned manually with the sequence of the selectivity filter of KvAP (T196–G200). Since the pore helix of KvAP (V183–A194) is preceding the selectivity filter on the N terminal side, the alignment includes this segment (Fig. 1). Thus, sequence T4881–G4898 of the target matches the section of KvAP. The sequences of the inner helix S6 of KvAP and the sequence F4921–K4951 of the target are aligned manually in order to match G4934 of RyR1 and G220 of KvAP, since G4934 is part of a GXXXXA motif [7,9,44] that is often found in potassium channels as a gating hinge [45]. The corresponding alanine of this motif of KvAP is replaced by a threonine (T225). Structure and sequence comparison with other potassium channels however show that G220 is at the gating hinge position (data not shown). Since the loop regions of the pore of RyR1 and KvAP differ considerably in length, homology modeling and sequence alignments are not done for these regions.

The homology modeling is performed in three steps. In the first step the selectivity filter and the four copies of the pore helices (T4881–G4898) are modeled simultaneously. Two Ca^{2+} ions are positioned in the selectivity filter according to the 1,3 configuration of K^{+} ions in the selectivity filter of potassium channels [46]. In the second step the four copies of the inner helices (F4921–K4951) are built around the four pore helices from step 1. In the third step the four copies of the outer helices (K4835–F4859) are modeled around the structure derived from the first two steps. The final homology model is consequently submitted to a series of energy minimizations.

A large number of loop models connecting the selectivity filter and the inner helix (D4899–F4920) of one of the four monomers are generated. During the calculations the homology model and an implicit membrane environment are taken into account. The loop models are divided into clusters according to a RMS criteria of 3 Å (Fig. 2A). Finally the highest scoring loop model of the largest cluster is chosen (cluster 0, Fig. 2A). Copying and insertion of the three other identical loops does not result in major steric clashes amongst neighboring loops. The low

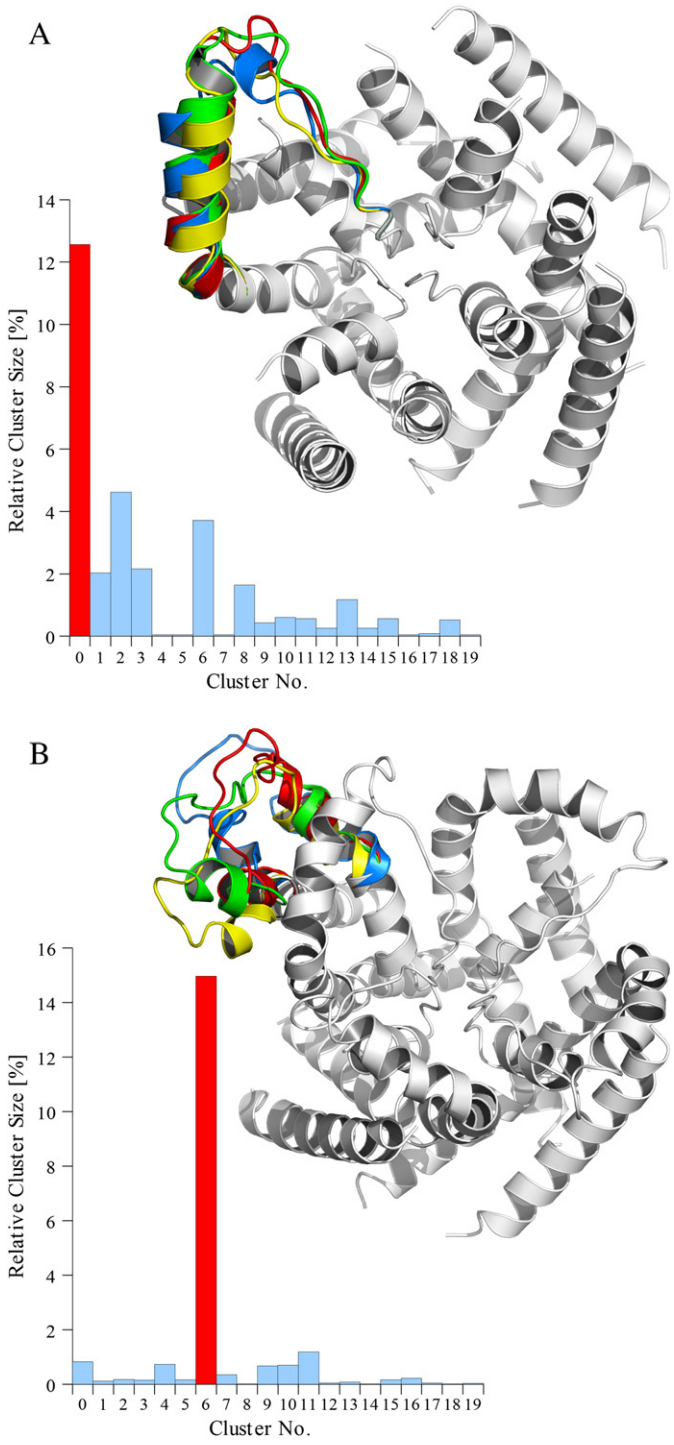

Fig. 2. Relative cluster sizes and highest scoring loop models connecting selectivity filter and inner helix (A) and outer helix and pore helix (B). The four highest scoring loop models of the largest cluster are shown in red, blue, green and yellow cartoon representation. During the loop generation the structure illustrated in white cartoon representation is present.

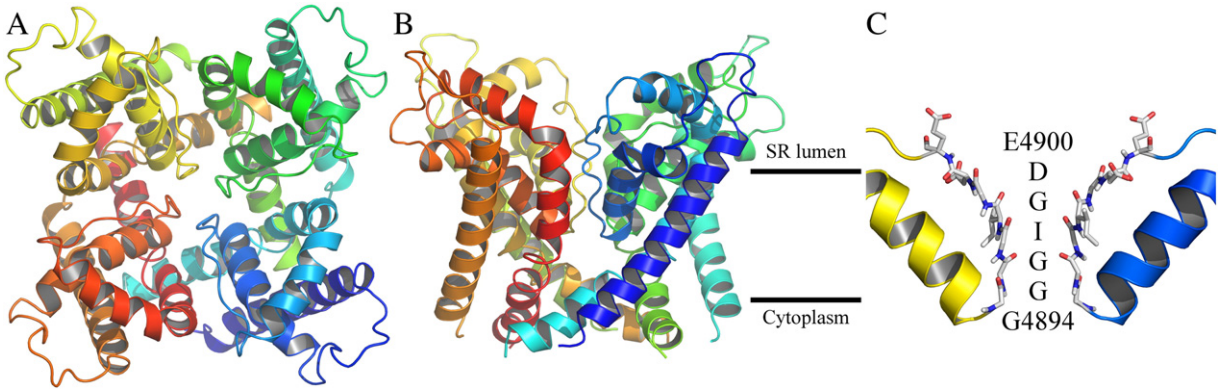

Fig. 3. The final model of the pore region of the RyR1. A top view from the luminal side (A) and a side view (B) of the model are shown in cartoon representation. (C) The pore helices of two monomers are shown in carton representation while the selectivity filter is illustrated in stick representation.

structural diversity is visualized presenting the four best scoring loops of cluster 0 in various colors (Fig. 2A). The loops are modeled as a helix from residues D4907 to F4920 and unstructured from residues D4899 to G4906. The orientation of the helix is parallel to the membrane surface.

The four inserted loops are present when generating the loop models connecting the outer helix and the pore helix (R4860–M4880) of one of the four monomers. The loop models are assigned to clusters using a RMS criteria of 3.3 Å (Fig. 2B). Smaller cluster radii do not result in any major cluster. The loop model with the best score from the biggest cluster is chosen (cluster 6, Fig. 2B), copied and inserted into the monomers as mentioned before. The modeled loop contains two short helices including residues R4860, K4861 and C4876–M4880. The final energy-minimized model of the pore region of the RyR1 is used in MD simulation studies on structure–function correlation (Fig. 3).

The final model fits into the shape obtained by cryo-EM for the respective protein [7,9] (Fig. 4). Especially the short helix (D4907–F4920) in the extramembrane region is found to be within the volume of the EM shape. The helix is amphipathic since the hydrophilic residues E4910, R4913 and D4917 all point towards the aqueous phase (Fig. 4D). The residues D4907 and E4908 at the N terminal end of the helix point away from the luminal pore entry. The residue D4878 is located in the

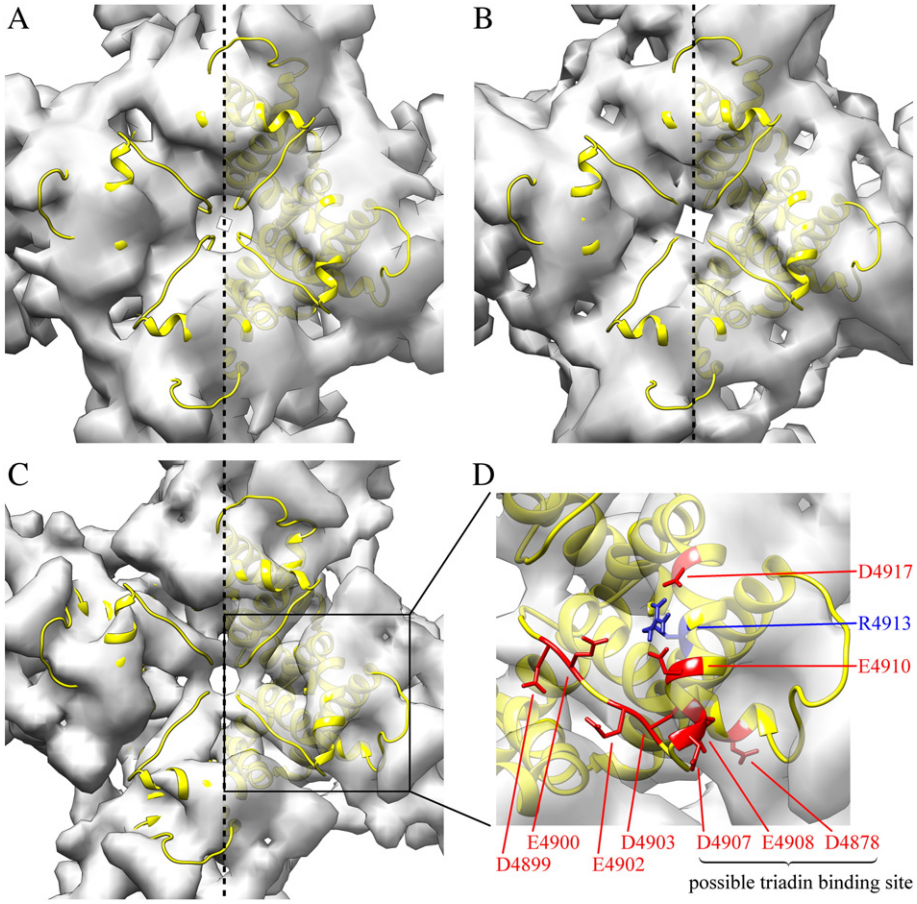

Fig. 4. The modeled pore region of RyR1 fitted in three cryo-EM density maps. The pore model is exhibited in yellow cartoon representation and fitted into three cryo-EM density maps that were obtained in two different studies and show the RyR1 in the closed (A) and open (B) state [9] and in the closed state (C) [7]. The charged residues of the loop connecting selectivity filter and inner helix are depicted in a magnification of one of the identical monomers (D). Furthermore the residue D4878 is shown since the residues D4878, D4907 and E4908 provide a possible triadin binding site [47].

vicinity of D4907 and E4908. These three negatively charged residues are known to be important for the binding of triadin to RyR1 [47] and therefore present a possible triadin binding site of the pore model (Fig. 4D).

3.2. MD simulations

Visual inspection of the MD trajectories of calcium ions suggest that the luminal pore entry of the model of the RyR1 is preferably occupied by a single calcium ion surrounded by four other calcium ions (Fig. 5). Furthermore the vestibule is occupied by one calcium ion. A top view from the luminal side (Fig. 5A) and a side view (Fig. 5B) of the spatial distribution function for calcium ions is shown in form of an isomesh with a contour level of 1 Ca^{2+}/nm^3. The spatial distribution function shown in Fig. 5A is displayed only for the luminal side of the RyR1, and in Fig. 5B it is illustrated only for the area parallel to the image plane in a range of ±0.5 nm from the pore axis. The corresponding two-dimensional calcium ion distributions exhibit a region of high probability density (HPD) (~2–6 Ca^{2+}/nm^2) at the luminal pore entry (Fig. 5C (top view) and D (side view)). This region is surrounded symmetrically by four HPD areas (>6 Ca^{2+}/nm^2) that are connected with the central region of HPD *via* areas of lower values (<2 Ca^{2+}/nm^2, Fig. 5C, D). The region of HPD corresponding to the calcium ion in the vestibule is an isolated spot, indicating that the calcium ion is 'trapped' (Fig. 5D).

In order to identify residues of the RyR that are important for the observed calcium ion distribution, the distance between every protein atom to the closest calcium ion in every frame is calculated and averaged over all frames (Fig. 5A, B). These average distances are averaged again for the four monomers. A4893 shows the smallest average distance to the calcium ion in the vestibule (0.64 ± 0.06 nm). Residues facing the lumen with an average distance of less than 0.7 nm are G4898 (0.66 ± 0.02 nm), D4899 (0.55 ± 0.03 nm), E4900 (0.60 ± 0.06 nm), E4902 (0.70 ± 0.12 nm), E4908 (0.65 ± 0.11 nm) and D4917 (0.64 ± 0.09 nm). G4898 and D4899 of these residues are in close contact with the ions occupying region A (see Fig. 7A) and D4899, E4900, E4902 and D4917 are in close contact with the ions occupying the regions B_i (see Fig. 7A) which is shown by average distance calculations for the individual regions. The residues A4893, D4899, E4900 and D4917 that exhibit an average distance of less than 0.65 nm and are in close contact with ions occupying region A, B_i or the vestibule are illustrated (Fig. 5A, B). The backbone carbonyl oxygens of alanine and glycine and the oxygens of the carboxyl group of aspartic acid and glutamic acid are the atoms with the smallest average distances to calcium ions.

The RDF of calcium ions at the luminal side of the RyR1 around the pore axis (Fig. 6) exhibits a first and a second maximum corresponding to the region of HPD at the luminal pore entry and the four surrounding HPD areas (Fig. 5C and D), respectively. On average one calcium ion is present within a radius of 0.46 nm around the pore axis (first maximum of RDF) and four more (second maximum of RDF) calcium ions occupy the region within a radius of 1.50 nm around the pore axis (Fig. 6).

The low-pass filtered trajectories of the four calcium ions with the largest occupancy times at the luminal pore entry show that diffusion occurs on the protein surface (Fig. 6). In order to further characterize the calcium ion dynamics on the luminal side of the RyR, this region is subdivided into region A, B_1, B_2, B_3 and B_4 corresponding to the regions of HPD (Fig. 7A, see also Fig. 6). Region A is defined as the cylinder with a radius of 0.46 nm around the pore axis and one fourth of the cylinder with a radius of 1.50 nm around the pore axis excluding region A constitutes one of the regions B_i. In addition, region C is defined as the cylinder with a radius of 1.50 nm around the pore axis proceeding from the regions A and B_i. Calcium ions that are not present in any of the defined regions are assigned to region D. The assignment of calcium ions to the regions A, B_1, B_2, B_3, B_4, C and D as a function of time is plotted (Fig. 7B). Several transitions of calcium ions between the defined regions can be observed. Diffusion occurs predominantly between the regions C/D and B_i and between the regions B_i and A. Fig. 7C shows a

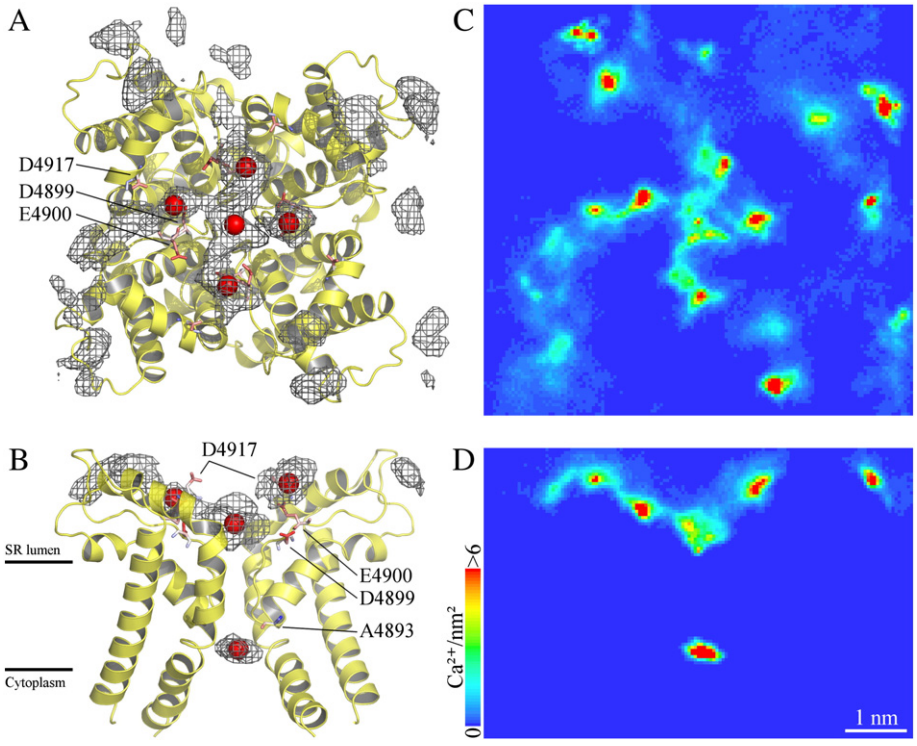

Fig. 5. Modeled pore region of the RyR1 and calcium ion distributions. A top view from the luminal side (A) and a side view (B) of the model are shown in yellow cartoon representation. The average positions of calcium ions occupying the luminal pore entry and the vestibule are depicted by red spheres. Residues with a small average distance to these calcium ions are displayed; colors represent the average distance of each atom (red–white–blue). The spatial distribution function for calcium ions is illustrated in form of an isomesh. The top view (C) and side view (D) of the corresponding two-dimensional distributions are shown. The regions of high probability density (HPD) match with the average positions of calcium ions.

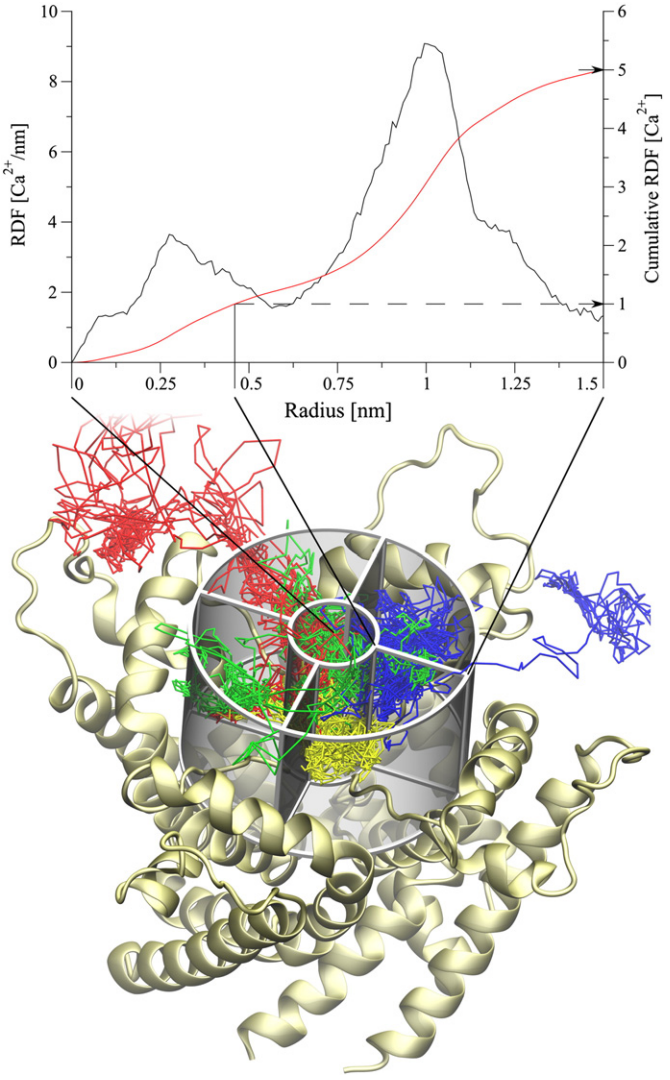

Fig. 6. Radial distribution function (RDF) of calcium ions and calcium ion trajectories at the luminal pore entry of the RyR1. The RDF around the pore axis has two maxima (black line). According to the cumulative RDF (red line), one calcium ion occupies the cylinder with a radius of 0.46 nm around the pore axis and five (=1 + 4) calcium ions are present in the cylinder with a radius of 1.50 nm. The model of the pore region of the RyR1 is shown in pastel yellow cartoon representation. The low-pass filtered trajectories of four calcium ions (yellow, green, blue and red) are illustrated.

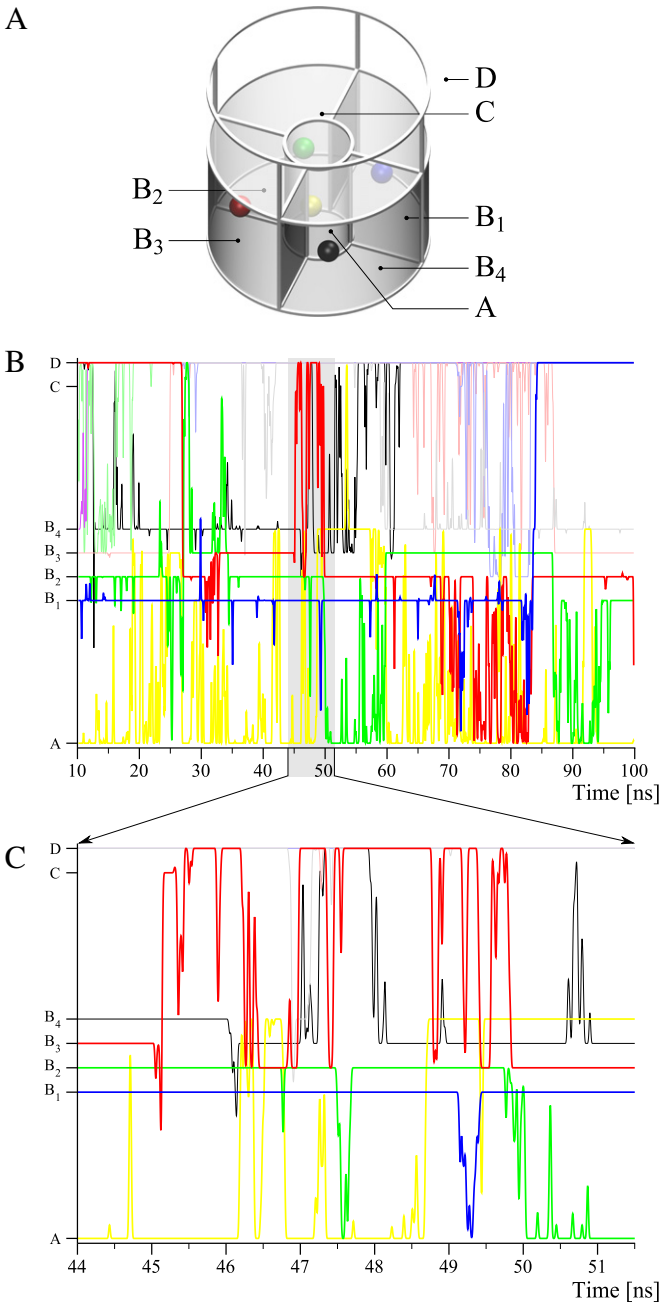

Fig. 7. Assignment of calcium ions to sub-regions. (A) The cylinder with a radius of 0.46 nm around the pore axis is defined as region A and the regions B_1, B_2, B_3 and B_4 as one fourth of the cylinder with a radius of 1.50 nm. The proceeding cylinder is defined as region C. Calcium ions that are not present in any of these regions are assigned to region D. Colored spheres depict the positions of five calcium ions at ~44 ns. The assignment of calcium ions to the defined regions as a function of time is shown (B). A magnification of an exemplary section is exhibited (C). The curves are smoothed using a Gaussian smoothing window (σ_B = 50 ps, σ_C = 10 ps).

magnification of an exemplary section of Fig. 7B. The calcium ion occupying the luminal pore entry (yellow line, region A) shifts to region B_4 at ~48.7 ns followed by a short occupancy of region A by the calcium ion shifting from region B_1 (blue line). At ~50 ns another calcium ion shifts from region B_2 to region A (green line) followed by the transition of a calcium ion from region D to region B_2 (red line). The trajectories show that calcium ions at the luminal pore entry (region A) are likely exchanged along the protein surface (*via* region B_i) and only unlikely *via* region C. Furthermore the regions A, B_1, B_2, B_3 and B_4 are typically occupied by a single calcium ion. They are ~10% of the time unoccupied and to ~80% and ~10% occupied with either one or two and more calcium ions, respectively (Table 1).

A PMF profile for a calcium ion at the luminal pore entry is derived along the axial direction (z) which allows the calcium ion to move freely in the x–y plane (Fig. 8). The average positions of the calcium ion of the single umbrella sampling windows are located at the protein surface (Fig. 8B, C) and coincide with the regions of HPD (Fig. 5C, D). The calculation of the average positions of the calcium ion allows assigning each umbrella sampling window to the above defined regions A–D (Fig. 7A) and thus assigning the regions A–D to the PMF profile (Fig. 8A). The regions A and B_i are separated by a small energy barrier (~2–3 kJ/mol). Within these regions only smaller energy barriers (~1–2 kJ/mol) occur. It is energetically less favorable (~5–15 kJ/mol) for the calcium ion to move to region D.

3.3. Sequence analysis

The alignments of the RyR1 and RyR2 and the application of TM prediction programs reveal a superposition of the TMDs of the RyR1 and the RyR2 (Fig. 9). Almost each of the TMDs M4a, M4b, M5, M6, M7a,

Table 1
Calcium ion occupancy at the luminal pore entry of the modeled pore region of the RyR1. The regions A, B_1, B_2, B_3 and B_4 are predominantly occupied by a single calcium ion. The cumulative average occupancy of the regions A, B_i and C is 5.00 by definition since the (cumulative) RDF is calculated for these regions.

Region	Average occupancy	Relative simulation time with an occupancy of		
	$\overline{N}_{Ca^{2+}}$ [1]	$N_{Ca^{2+}} = 0$ [%]	$N_{Ca^{2+}} = 1$ [%]	$N_{Ca^{2+}} \geq 2$ [%]
A	1.00	13.6	73.4	13.0
B_1	0.91	12.6	83.6	3.8
B_2	0.99	8.3	84.8	6.9
B_3	1.04	9.0	77.7	13.3
B_4	1.02	5.8	86.1	8.1
C	0.04	96.5	3.5	0.04

M7b, M8 and M10 of the RyR1 (according to [10,11]) are aligning with the predicted TM regions. All TM prediction programs identify M5, M6, M8 and M10 as TMDs of both, the RyR1 and the RyR2. The region M4a/b of the RyR1 is predicted as a hairpin loop by all programs except SOSUI. While the programs TMHMM2, SOSUI and SVMtm predict only one TMD for the corresponding region of the RyR2, the programs Phobius, HMMTOP, OCTOPUS and MEMSAT-SVM also predict a hairpin loop. The region M7a/b of the RyR1 is identified as hairpin loop by OCTOPUS and MEMSAT-SVM and as single TMD by the other programs. While Phobius, OCTOPUS and MEMSAT-SVM predict a hairpin loop for the corresponding region of the RyR2, other programs identify only one TMD. The region M4233–S4260 of the RyR2 is predicted to be transmembrane by TMHMM2, SOSUI, SVMtm, Phobius and HMMTOP, while none of the used programs identifies any TMD in the corresponding region of the RyR1.

The program ClustalW2 aligns TMD1 of 2B from coxsackie virus and poliovirus with M4b of the human RyR2. The alignment does not exhibit any gaps in the sequences. TMD1 of 2B from coxsackie virus is partially aligned with M7b of the RyR1. TMD1 of 2B from poliovirus is aligned with a non-TM region of the RyR1. TMD2 of 2B from coxsackie virus and poliovirus is aligned with M6 of the RyR1 and the RyR2. As a result of the alignment, 2B from both poliovirus and coxsackie virus shows sequence identity with the outer helices of the human RyR2. The alignment of the RyR1 and the RyR2 shows that the two isoforms share lower sequence identity in the M4 region where TMD1 of 2B is aligned with the human RyR2, while the sequence of the RyR1 and the RyR2 is highly conserved in the putative pore region (M8–M10).

4. Discussion

Our model of the pore region of the RyR1 presented in this study is constructed based on the architecture of potassium channels. The arrangement of outer, inner and pore helices and of the selectivity filter is therefore similar to that of other pore models of RyR that also adopt the structure of potassium channels [34,44,48]. The proposed structures of the luminal loops of those models, that connect selectivity filter and inner helix and outer helix and pore helix, differ, however, from our model. The corresponding loops of potassium channels are substantially shorter than those of RyRs and therefore do not provide a promising template. Especially the structure of the loop connecting selectivity filter and inner helix is of great importance as mutations of amino acids in this region significantly alter channel function [43,49,50]. In our pore model, part of this loop is modeled as an amphipathic helix (D4907–F4920) that is found to fit in available cryo-EM density maps of RyR1 [7,9]. Our proposed structure of this amphipathic helix with the proceeding inner helix might explain why TM prediction programs do not identify the proposed inner helix [7,9,44] as TMD but identify the TMD in a more central position of amphipathic and inner helix. The residues D4907 and E4908 are located at the N terminal end of the amphipathic helix and provide a possible binding site for triadin together with D4878. The unequal contribution of these three residues to triadin binding (D4907 > E4908 > D4878) [47] equals their axial positions in our model: $z_{D4907} > z_{E4908} > z_{D4878}$.

A ring of four negatively charged amino acids (D4899) is located directly at the pore entry of our model. Four negatively charged amino acids (the EEEE/EEDD locus) also play a key role in the function of voltage-gated calcium channels [51]. An atomistic model of the outer vestibule of the N-type calcium channel places these four glutamate residues in the selectivity filter [52]. These positions are similar but located more central in the selectivity filter compared to the arrangement of the four aspartic residues in our pore model of RyR1. In contrast to our model of the homotetrameric RyR1, the charged amino acids of the N-type calcium channel model are arranged asymmetrically due to the architecture of voltage-gated calcium channels with four homologous but unequal subunits [52]. Furthermore the model of the outer vestibule of the N-type calcium channel [52] shows a remarkably lower number of negatively charged amino acids in comparison to our model of RyR1.

Modeling the pore region of the RyR1 with atomic detail allows the proposal of structural elements and of the locations of key residues. In other studies, a simplified model of the pore of RyR reduced on a small number of important residues has been constructed [53,54]. The simplified model has been able to reproduce current/voltage curves, the anomalous mole fraction effect and ion selectivity [53,54]. It is, however, the goal to elucidate the atomic structure of the RyR in order to conduct simulations in full atomic detail.

The performed MD simulations in our study reveal a HPD of calcium ions in the vestibule and at the luminal pore entry of the RyR1 which has been reported earlier [34]. In our study the dynamics and a detailed distribution of calcium ions around the luminal pore entry are reported. The observation of a calcium ion occupying the luminal pore entry

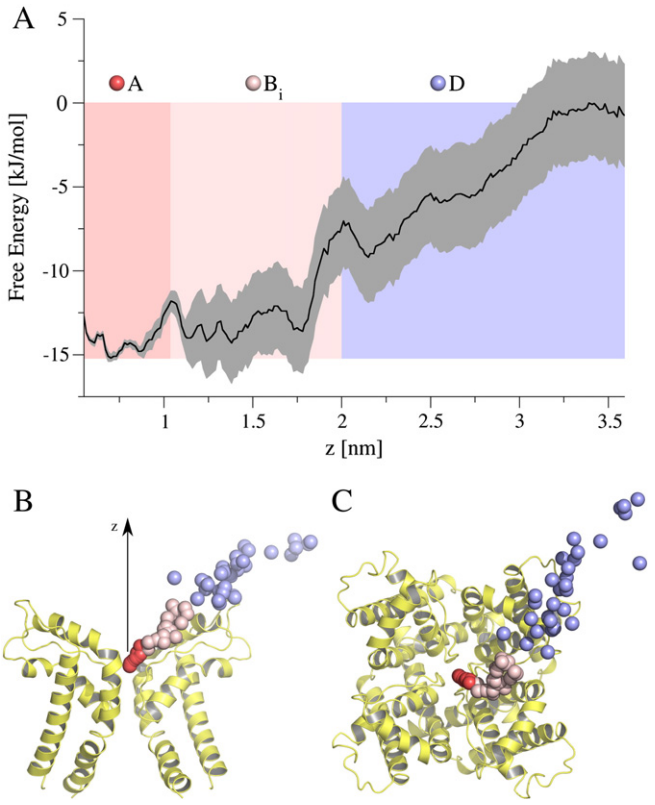

Fig. 8. PMF profile for Ca^{2+} at the luminal pore entry. (A) The above defined regions A, B_i and D are assigned to the PMF profile. Regions A and B are energetically more favorable for the calcium ion than region D and are separated by a small energy barrier. A side view (B) and a top view (C) of the average positions of the calcium ion of the single umbrella sampling windows and the pore model are shown. The model is shown in yellow cartoon representation and the positions of the calcium ion are depicted by spheres that are colored according to the regions A, B_i and D. Jumps of the calcium ion between the four symmetrical branches were removed before calculating the average positions.

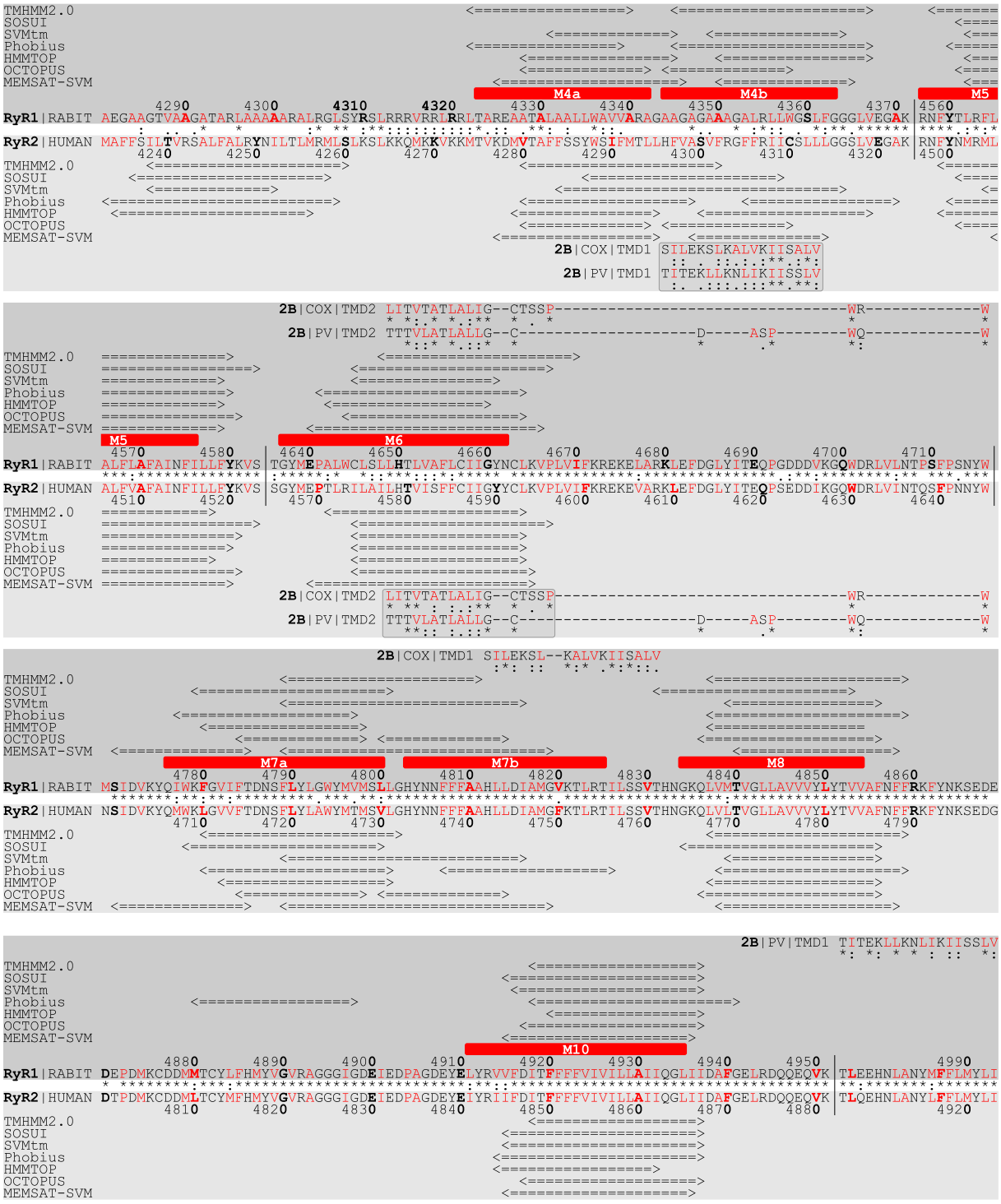

Fig. 9. Sequence alignment of the RyR1, RyR2 and TMDs of 2B from coxsackie virus (COX) and poliovirus (PV). The symbols denote the following: '*' = identical residues, ':' = conserved substitution and '.' = semi-conserved substitution. Hydrophobic, aromatic (not Y) and small residues (AVFPMILW) are depicted in red according to ClustalW2. The predicted TM regions of the RyR1 and RyR2 are marked with '<= =>'. Red bars indicate the TMDs M4a, M4b, M5, M6, M7a, M7b, M8 and M10 of the RyR1 according to [10,11]. The sequence alignments of the TMDs of 2B with predicted TMDs of the cardiac RyR2 are boxed.

(region A) and the four additional calcium ions surrounding it (regions B_i) suggest an efficient mechanism of calcium ion supply to the luminal pore entry. It has been stated earlier that a high density of acidic residues on the RyR surface is likely to contribute to calcium channel function [44]. The local calcium concentration in vicinity to the luminal protein surface is likely increased due to the negatively charged amino acids facing the lumen. Our conducted MD simulations demonstrate that the arrangement of amino acids in the modeled pore region of the RyR1 limits the diffusion pathway of calcium ions in close vicinity to the luminal pore entry. In the L-type calcium channel, it has been found that a calcium ion is bound in the selectivity filter and permeates the channel when a second calcium ion enters the filter [55,56]. A similar process with the four additional calcium ions from the regions B_i might take place in the RyR. Our PMF calculations demonstrate that the regions A and B_i are only separated by a small energy barrier. Although the permeation of calcium ions is not observed in our conducted

MD simulations, we suggest that the selectivity filter of the RyR is traversed by a calcium ion from region A while another calcium ion crosses the small energy barrier and shifts from one of the regions B_i to region A. Simultaneously another calcium ion might enter the regions B_i from region D. We propose that the restricted diffusion of calcium ions along the four branches to the center of the luminal pore entry constitutes an efficient mechanism of calcium ion supply and thus enhances calcium ion conductance of the RyR.

Average distance calculations indicate that the calcium ion in the vestibule is in closest contact with A4893 of our model of the pore region of the RyR1. Experimental mutagenesis studies demonstrated that the residues D4938 and D4945 of the RyR1 are important for channel function [57]. These two residues are part of the inner helices in the region of the vestibule of our modeled pore region. Thus, the acidic residues D4938 and D4945 might be involved in the immobilization of the calcium ion in the vestibule, while the contact with A4893 might also be due to the vestibule geometry. According to our average distance calculations, the acidic residues D4899, E4900, E4902 and D4917 are in close contact with calcium ions occupying the regions A and B_i. Mutagenesis experiments showed that the neutralization of D4899, E4900 or D4917 essentially alters calcium ion conductance of the RyR1 [43,49]. The neutralization of E4902 did not show major changes in channel function [43] however the double neutralization ED4832AA in RyR2 equivalent to ED4902AA in RyR1 exhibited a significant impact [50]. These experimental findings are consistent with our identification of negatively charged amino acids at the luminal pore entry that are important for calcium channel function, since E4902 depicts a larger average distance to calcium ions than D4899, E4900 and D4917. We suggest that the neutralization of these acidic residues alters the calcium ion dynamics at the luminal pore entry and perturbs the supply of calcium ions.

Activity of a receptor can be modulated by interaction with ligands and, as a consequence of the interaction, ion homeostasis within subcellular locations is altered. This could also be done by integrating 'wrong' parts into the receptor during assembly. 'Wrong' parts could be those, which are just similar but not identical to the 'original' parts. This scenario as a mode of action is proposed to be adopted by the viral channel forming protein Vpu of HIV-1 [19]. It is proposed that Vpu interacts with acid sensitive K^+ channels (TASK) due to sequence similarity [19]. Driven by this proposal, we perform sequence alignments of 2B of coxsackie and polioviruses with RyR1 and RyR2. The enormous size of the RyR reflects its ability to interact with many other modulating proteins [6]. TMD1 of 2B is aligned with M4b of the human RyR2 which is a region of lower sequence homology with the RyR1. The lower sequence identity might indicate that this region is responsible for a specific modulation of the RyR2 in cardiac muscle cells. Furthermore with 2B expressed in an infected cell the protein might replace respective TMDs of the RyR2 leading to a structurally and functionally 'miss-manufactured' channel. Consequently calcium homeostasis would be affected. It would be important but challenging to test this hypothesis experimentally.

5. Conclusions

An atomistic pore model of RyR is constructed based on the structure of potassium channels. Part of the loop connecting selectivity filter and inner helix is modeled as amphipathic helix, resulting in a plausible arrangement of charged amino acids around the luminal pore entry.

MD simulations suggest that calcium ions are channeled *via* the protein surface to the luminal pore entry of the RyR. The calcium ion conductance of RyRs is likely increased due to this mechanism of calcium ion supply.

Based on a bioinformatics approach it is hypothesized that 2B from coxsackie virus might interfere with the assembly of the cardiac RyR by replacing TMDs of the RyR and thus interfere with calcium homeostasis of infected cells.

Acknowledgements

WBF thanks the National Science Council for financial support (NSC101-2112-M-010-002-MY3). RF, WBF and RS gratefully acknowledge the German Academic Exchange Service (DAAD) for their financial support. RS was granted a Ph.D. scholarship of the Heidelberg Medical School and the Baden-Württemberg-STIPENDIUM. RF thanks for the financial support by the German Excellence Initiative II — Global Networks.

References

[1] Y. Zhou, T.K. Frey, J.J. Yang, Viral calciomics: interplays between Ca^{2+} and virus, Cell Calcium 46 (2009) 1–17.
[2] C. Brisac, F. Teoule, A. Autret, I. Pelletier, F. Colbere-Garapin, C. Brenner, C. Lemaire, B. Blondel, Calcium flux between the endoplasmic reticulum and mitochondrion contributes to poliovirus-induced apoptosis, J. Virol. 84 (2010) 12226–12235.
[3] R. Zalk, S.E. Lehnart, A.R. Marks, Modulation of the ryanodine receptor and intracellular calcium, Annu. Rev. Biochem. 76 (2007) 367–385.
[4] J.T. Lanner, D.K. Georgiou, A.D. Joshi, S.L. Hamilton, Ryanodine receptors: structure, expression, molecular details, and function in calcium release, Cold Spring Harb. Perspect. Biol. 2 (2010) a003996.
[5] M. Mosqueira, U. Zeiger, M. Förderer, H. Brinkmeier, R.H. Fink, Cardiac and respiratory dysfunction in Duchenne muscular dystrophy and the role of second messengers, Med. Res. Rev. 33 (2013) 1174–1213.
[6] F. Van Petegem, Ryanodine receptors: structure and function, J. Biol. Chem. 287 (2012) 31624–31632.
[7] S.J. Ludtke, I.I. Serysheva, S.L. Hamilton, W. Chiu, The pore structure of the closed RyR1 channel, Structure 13 (2005) 1203–1211.
[8] M. Samso, T. Wagenknecht, P.D. Allen, Internal structure and visualization of transmembrane domains of the RyR1 calcium release channel by cryo-EM, Nat. Struct. Mol. Biol. 12 (2005) 539–544.
[9] M. Samso, W. Feng, I.N. Pessah, P.D. Allen, Coordinated movement of cytoplasmic and transmembrane domains of RyR1 upon gating, PLoS Biol. 7 (2009) e85.
[10] G.G. Du, B. Sandhu, V.K. Khanna, X.H. Guo, D.H. MacLennan, Topology of the Ca^{2+} release channel of skeletal muscle sarcoplasmic reticulum (RyR1), Proc. Natl. Acad. Sci. U. S. A. 99 (2002) 16725–16730.
[11] G.G. Du, G. Avila, P. Sharma, V.K. Khanna, R.T. Dirksen, D.H. MacLennan, Role of the sequence surrounding predicted transmembrane helix M4 in membrane association and function of the Ca(2+) release channel of skeletal muscle sarcoplasmic reticulum (ryanodine receptor isoform 1), J. Biol. Chem. 279 (2004) 37566–37574.
[12] G. Orthopoulos, K. Triantafilou, M. Triantafilou, Coxsackie B viruses use multiple receptors to infect human cardiac cells, J. Med. Virol. 74 (2004) 291–299.
[13] F.J.M. van Kuppeveld, J.G.J. Hoenderop, R.L.L. Smeets, P.H.G.M. Willems, H.B.P.M. Dijkman, J.M.D. Galama, W.J.G. Melchers, Coxsackievirus protein 2B modifies endoplasmic reticulum membrane and plasma membrane permeability and facilitates virus release, EMBO J. 16 (1997) 3519–3532.
[14] F.J.M. van Kuppeveld, W.J.G. Melchers, K. Kirkegaard, J.R. Doedens, Structure–function analysis of Coxsackie B3 virus protein 2B, Virology 227 (1997) 111–118.
[15] F.J.M. van Kuppeveld, J.M.D. Galama, J. Zoll, P.J.J.C. van den Hurk, W.J.G. Melchers, Coxsackie B3 virus protein 2B contains a cationic amphipathic helix that is required for viral RNA replication, J. Virol. 70 (1996) 3876–3886.
[16] A.S. de Jong, H.-J. Visch, F. de Mattia, M.M. van Dommelen, H.G. Swart, T. Luyten, G. Callewaert, W.J. Melchers, P.H. Willems, F.J. Van Kuppeveld, The coxsackievirus 2B protein increases efflux of ions from the endoplasmic reticulum and Golgi, thereby inhibiting protein trafficking through the Golgi, J. Biol. Chem. 281 (2006) 14144–14150.
[17] G. Patargias, T. Barke, A. Watts, W.B. Fischer, Model generation of viral channel forming 2B protein bundles from polio and coxsackie viruses, Mol. Membr. Biol. 26 (2009) 309–320.
[18] W.B. Fischer, Y.-T. Wang, C. Schindler, C.-P. Chen, Mechanism of function of viral channel proteins and implications for drug development, Int. Rev. Cell Mol. Biol. 294 (2012) 259–321.
[19] K. Hsu, J. Seharaseyon, P. Dong, S. Bour, E. Marbán, Mutual functional destruction of HIV-1 Vpu and host TASK-1 channel, Mol. Cell 14 (2004) 259–267.
[20] A. Krogh, B. Larsson, G. von Heijne, E.L. Sonnhammer, Predicting transmembrane protein topology with a hidden Markov model: application to complete genomes, J. Mol. Biol. 305 (2001) 567–580.
[21] T. Hirokawa, S. Boon-Chieng, S. Mitaku, SOSUI: classification and secondary structure prediction system for membrane proteins, Bioinformatics 14 (1998) 378–379.
[22] Z. Yuan, J.S. Mattick, R.D. Teasdale, SVMtm: support vector machines to predict transmembrane segments, J. Comput. Chem. 25 (2004) 632–636.
[23] L. Käll, A. Krogh, E.L. Sonnhammer, A combined transmembrane topology and signal peptide prediction method, J. Mol. Biol. 338 (2004) 1027–1036.
[24] G.E. Tusnady, I. Simon, The HMMTOP transmembrane topology prediction server, Bioinformatics 17 (2001) 849–850.
[25] H. Viklund, A. Elofsson, OCTOPUS: improving topology prediction by two-track ANN-based preference scores and an extended topological grammar, Bioinformatics 24 (2008) 1662–1668.
[26] T. Nugent, D.T. Jones, Transmembrane protein topology prediction using support vector machines, BMC Bioinforma. 10 (2009) 159.
[27] S.Y. Lee, A. Lee, J. Chen, R. MacKinnon, Structure of the KvAP voltage-dependent K^+ channel and its dependence on the lipid membrane, Proc. Natl. Acad. Sci. U. S. A. 102 (2005) 15441–15446.

[28] C. Wang, P. Bradley, D. Baker, Protein–protein docking with backbone flexibility, J. Mol. Biol. 373 (2007) 503–519.
[29] V. Yarov-Yarovoy, J. Schonbrun, D. Baker, Multipass membrane protein structure prediction using Rosetta, Proteins 62 (2006) 1010–1025.
[30] P. Barth, J. Schonbrun, D. Baker, Toward high-resolution prediction and design of transmembrane helical protein structures, Proc. Natl. Acad. Sci. U. S. A. 104 (2007) 15682–15687.
[31] S. Pronk, S. Pall, R. Schulz, P. Larsson, P. Bjelkmar, R. Apostolov, M.R. Shirts, J.C. Smith, P.M. Kasson, D. van der Spoel, B. Hess, E. Lindahl, GROMACS 4.5: a high-throughput and highly parallel open source molecular simulation toolkit, Bioinformatics 29 (2013) 845–854.
[32] G.E. Tusnády, Z. Dosztányi, I. Simon, TMDET: web server for detecting transmembrane regions of proteins by using their 3D coordinates, Bioinformatics 21 (2005) 1276–1277.
[33] M.G. Wolf, M. Hoefling, C. Aponte-Santamaría, H. Grubmüller, G. Groenhof, g_membed: efficient insertion of a membrane protein into an equilibrated lipid bilayer with minimal perturbation, J. Comput. Chem. 31 (2010) 2169–2174.
[34] S. Ramachandran, A.W. Serohijos, L. Xu, G. Meissner, N.V. Dokholyan, A structural model of the pore-forming region of the skeletal muscle ryanodine receptor (RyR1), PLoS Comput. Biol. 5 (2009) e1000367.
[35] L.D. Schuler, X. Daura, W.F. van Gunsteren, An improved GROMOS96 force field for aliphatic hydrocarbons in the condensed phase, J. Comput. Chem. 22 (2001) 1205–1218.
[36] J. Krüger, W.B. Fischer, Exploring the conformational space of Vpu from HIV-1: a versatile adaptable protein, J. Comput. Chem. 29 (2008) 2416–2424.
[37] I. Chandrasekhar, M. Kastenholz, R.D. Lins, C. Oostenbrink, L.D. Schuler, D.P. Tieleman, W.F. van Gunsteren, A consistent potential energy parameter set for lipids: dipalmitoylphosphatidylcholine as a benchmark of the GROMOS96 45A3 force field, Eur. Biophys. J. 32 (2003) 67–77.
[38] G.M. Torrie, J.P. Valleau, Nonphysical sampling distributions in Monte Carlo free-energy estimation: umbrella sampling, J. Comput. Phys. 23 (1977) 187–199.
[39] B. Corry, M. Thomas, Mechanism of ion permeation and selectivity in a voltage gated sodium channel, J. Am. Chem. Soc. 134 (2011) 1840–1846.
[40] S. Furini, C. Domene, On conduction in a bacterial sodium channel, PLoS Comput. Biol. 8 (2012) e1002476.
[41] J.S. Hub, B.L. de Groot, D. van der Spoel, g_wham—a free weighted histogram analysis implementation including robust error and autocorrelation estimates, J. Chem. Theory Comput. 6 (2010) 3713–3720.
[42] F. Zorzato, J. Fujii, K. Otsu, M. Phillips, N.M. Green, F.A. Lai, G. Meissner, D.H. MacLennan, Molecular cloning of cDNA encoding human and rabbit forms of the Ca^{2+} release channel (ryanodine receptor) of skeletal muscle sarcoplasmic reticulum, J. Biol. Chem. 265 (1990) 2244–2256.
[43] Y. Wang, L. Xu, D.A. Pasek, D. Gillespie, G. Meissner, Probing the role of negatively charged amino acid residues in ion permeation of skeletal muscle ryanodine receptor, Biophys. J. 89 (2005) 256–265.
[44] W. Welch, S. Rheault, D.J. West, A.J. Williams, A model of the putative pore region of the cardiac ryanodine receptor channel, Biophys. J. 87 (2004) 2335–2351.
[45] Y. Jiang, A. Lee, J. Chen, M. Cadene, B.T. Chait, R. MacKinnon, The open pore conformation of potassium channels, Nature 417 (2002) 523–526.
[46] Y. Zhou, J.H. Morais-Cabral, A. Kaufman, R. MacKinnon, Chemistry of ion coordination and hydration revealed by a K^+ channel-Fab complex at 2.0 A resolution, Nature 414 (2001) 43–48.
[47] S.A. Goonasekera, N.A. Beard, L. Groom, T. Kimura, A.D. Lyfenko, A. Rosenfeld, I. Marty, A.F. Dulhunty, R.T. Dirksen, Triadin binding to the C-terminal luminal loop of the ryanodine receptor is important for skeletal muscle excitation–contraction coupling, J. Gen. Physiol. 130 (2007) 365–378.
[48] S. Ramachandran, A. Chakraborty, L. Xu, Y. Mei, M. Samso, N.V. Dokholyan, G. Meissner, Structural determinants of skeletal muscle ryanodine receptor gating, J. Biol. Chem. 288 (2013) 6154–6165.
[49] L. Gao, D. Balshaw, L. Xu, A. Tripathy, C. Xin, G. Meissner, Evidence for a role of the lumenal M3–M4 loop in skeletal muscle Ca(2+) release channel (ryanodine receptor) activity and conductance, Biophys. J. 79 (2000) 828–840.
[50] F.C. Mead-Savery, R. Wang, B. Tanna-Topan, S.R. Chen, W. Welch, A.J. Williams, Changes in negative charge at the luminal mouth of the pore alter ion handling and gating in the cardiac ryanodine-receptor, Biophys. J. 96 (2009) 1374–1387.
[51] W.A. Sather, E.W. McCleskey, Permeation and selectivity in calcium channels, Annu. Rev. Physiol. 65 (2003) 133–159.
[52] R. Chen, S.H. Chung, Complex structures between the N-type calcium channel (CaV2.2) and omega-conotoxin GVIA predicted via molecular dynamics, Biochemistry 52 (2013) 3765–3772.
[53] D. Gillespie, Energetics of divalent selectivity in a calcium channel: the ryanodine receptor case study, Biophys. J. 94 (2008) 1169–1184.
[54] D. Gillespie, L. Xu, Y. Wang, G. Meissner, (De)constructing the ryanodine receptor: modeling ion permeation and selectivity of the calcium release channel, J. Phys. Chem. B 109 (2005) 15598–15610.
[55] B. Corry, T.W. Allen, S. Kuyucak, S.H. Chung, Mechanisms of permeation and selectivity in calcium channels, Biophys. J. 80 (2001) 195–214.
[56] B. Corry, T. Vora, S.H. Chung, Electrostatic basis of valence selectivity in cationic channels, Biochim. Biophys. Acta 1711 (2005) 72–86.
[57] L. Xu, Y. Wang, D. Gillespie, G. Meissner, Two rings of negative charges in the cytosolic vestibule of type-1 ryanodine receptor modulate ion fluxes, Biophys. J. 90 (2006) 443–453.